Harnessing Luminescence from Heavy Atom-Free Organic Charge Transfer Cocrystal

Suvarna Sujilkumar,[a] and Mahesh Hariharan[a]*

School of Chemistry, Indian Institute of Science Education and Research Thiruvananthapuram, Vithura, Thiruvananthapuram, Kerala, India 695551

Supporting Information (SI)

Contents

Section A: Materials and Methods

All chemicals were obtained from commercial suppliers and used as received without further purification. The reaction was carried out in oven-dried glassware before use and, wherever necessary, was performed under dry nitrogen in dried, anhydrous solvents using standard gastight syringes, cannula, and septa. Solvents were dried and distilled by standard laboratory purification techniques. TLC analyses were performed on silica gel 60 F254 plates (0.25 mm, Merck), and developed TLC plates were visualized under short and long-wavelength UV lamps. Flash column chromatography was performed using silica gel of 200-400 mesh employing a solvent polarity correlated with the TLC mobility observed for the substance of interest. Yields refer to chromatographically and spectroscopically homogenous substances. ^{1}H NMR spectrum was measured on a 500 MHz Bruker avance DPX spectrometer. The internal standard used for ^{1}H NMR is tetramethyl silane (TMS). Mass spectra were obtained using a Bruker UltrafleXtreme MALDI-TOF/TOF with Matrix-Assisted Laser Desorption/Ionization (MALDI, positive mode). FTIR spectra (with the spectral resolution of 4 cm^{1}) were collected on a Shimadzu IRPrestige-21 FTIR spectrometer by using KBr pellet method.

1.1 Spectroscopy Experimental Details

Kubelka-Munk absorption recorded on UV-Vis-NIR Perkin Elmer Lambda 950 spectrometer respectively. Kubelka-Munk transformed reflectance spectra in the crystalline state were measured in the diffuse reflectance mode. The Kubelka-Munk model is quite accurate when the particle size is smaller or similar to the wavelength of the excitation.[1] The diffuse reflectance spectra allow no separation of the reflection, refraction, and diffraction occurring from the crystalline samples. As a result, the diffuse reflectance spectra are not as sensitive compared to the UV-vis absorption spectra and can possibly be broader as compared to the typical absorbance and fluorescence excitation spectra.

Photoluminescence Measurements: Emission measurements were carried out using Horiba Jobin Yvon Fluorolog spectrometer. Photoluminescence measurements of crystals were performed by carefully preparing the sample with an optimized number of sub-millimeter-sized crystals and placing it at a designated orientation, wherein self-absorption could be attenuated.[2] Temperature-dependent photoluminescence measurements of crystals were performed by Edinburgh FLS1000 fluorescence spectrophotometer equipped with a cryostat. The sample was mixed with KBr and made into pellets used for temperature-dependent emission measurement by exciting at 350 nm. Gated emission measurements were carried out using Horiba Jobin Yvon Fluorolog spectrometer equipped with flash lamp of pulse-width of 3 μs. Temperature-dependent (90K-300K) gated measurements were carried out using liquid nitrogen cryostat (Janis VNF-100). The crystal was sandwiched between two quartzs pieces for the measurements.

Lifetime Measurements: The temperature-dependent lifetime measurements at vacuum were obtained on the Edinburgh FLS1000 fluorescence spectrophotometer equipped with 405 nm diode laser and collected at 577 nm equipped with cryostat (20 K-300 K) under vacuum. The crystal was sandwiched between two quartzs pieces for the measurements. Photoluminescence quantum yield was recorded using an integration sphere in the FLS1000 fluorescence spectrophotometer.

Photoluminescence lifetime measurements of PYDB were carried out using picosecond Time-Correlated Single-Photon Counting (TCSPC) system from Horiba Jobin Yvon-IBH. A pulsed diode laser (NanoLED-310L) of 310 nm wavelength with a pulse width of less than 1 ns was used to excite the samples. The photons from the sample were introduced into a monochromator (5000M) and detected using a

microchannel platephotomultiplier tube (MCP-PMT; Hamamatsu R3809U-50) having an instrument response time of 38.6 ps. Data station software controls TCSPC electronics (data station hub including Hub- NL, NanoLED controller) and detection unit. Colloidal silica solution is used for measuring the instrument response function. Fitting of luminescence decay and lifetimes are obtained using the fluorescence decay analysis software (DAS6.3).

The PL decay of all the samples was fitted with the biexponential decay model, and the goodness of fit was assessed from the χ^2 value (χ^2 = 1+0.25) and residual plot. Amplitude average lifetime (τ_{avg}) was obtained using the equation

$$\tau_{avg} = \frac{\alpha 1\tau 1+\alpha 2\tau 2}{\alpha 1+\alpha 2} \qquad \text{(Equation S1)}$$

where, τ and α are lifetime and pre-exponential factors of various components, respectively and subscripts 1 and 2, denote the components.

FLIM Measurements: Carefully handpicked one single crystal of PYDB-TCNB cocrystals are placed on a plasma-cleaned coverslip of 0.13-0.16 mm thickness to avoid the photon saturation of the SPAD detector. The coverslip sample was then kept in the microscope stage for measurements. The temperature and humidity of the room were kept at 22^{o}C and 40 %, respectively.

FLIM measurements of the PYDB-TCNB cocrystal were carried out using the MicroTime 200 (MT200) time-resolved confocal fluorescence microscope from PicoQuant, Germany. It includes an inverted microscope (Olympus IX83), a piezo scanning stage (P-733.2CD, PI), and a water immersion objective (UplanSApo 60X NA 1.2). PYDB-TCNB cocrystal was excited using a 405 nm pulsed laser (LDH-D-C-405, PicoQuant) with a pulse repetition rate of 5 MHz. The photons collected using the objective were spectrally filtered using a major dichroic mirror (zt405rdcUF3, Chroma) and a 425nm long-pass emission filter (Semrock). A 50 μm pinhole was used for the spatial filtering of photons and these photons were focused into a single-photon avalanche photodiode (SPAD) detector (Excelitas SPAD).

1.2 X-ray Crystallography

High-quality crystals of PYDB and PYDB-TCNB with appropriate dimensions were selected for the X-ray diffraction experiments. Crystallographic data collected are presented in Table S1. Single crystal was mounted using oil (Infineum V8512) on a glass fibre. All measurements were made on a CCD area detector with graphite monochromated Mo K_α radiation. The data was collected using Bruker APEXII detector and processed using APEX2 from Bruker. The structure was solved by direct method and expanded using the Fourier technique. The non-hydrogen atoms were refined anisotropically. Hydrogen atoms were included in idealized positions but not refined. Their positions were constrained relative to their parent atom using the appropriate HFIX command in SHELX-97.[3] All programs used during the crystal structure analysis are incorporated in the WINGX software.[4, 5] The full validation of CIF and structure factor was performed using the checkCIF utility and found to be free of major alert levels. 3D structure visualization and the exploration of the crystal packing were carried out using Mercury 3.10.1.[6, 7]

1.3 Computational Analysis

All the calculations are carried out in Gaussian 16.[8] The frontier molecular orbitals (FMO) of PYDB-TCNB were obtained from the generated cube files of energy calculations. TDDFT calculation is performed using LC-ωhPBE functional for the accurate prediction of CT character and def2svp basis set. Hole-electron analysis are carried out using Multiwfn version 3.7.[9] Electron and hole transfer coupling values were calculated by employing the CATNIP Tool version 1.9.[10] Both multiwfn and CATNIP use post-processed Gaussian 16 output files for the respective analyses.[10]

1.4 Noncovalent interaction (NCI) Plot[11]

NCI analysis employs an index based on electron density and its derivatives to identify noncovalent interactions. A two-dimensional plot of reduced electron density (*s*) against electron density (*ρ*) and the critical points are associated with the troughs appearing in the plot. Reduced electron density is given by:

$$s = \frac{1}{2(3\pi^2)^{1/3}} \frac{|\nabla\rho|}{\rho^{4/3}} \quad \text{(Equation S2)}$$

Noncovalent interactions occur in the real space points where these troughs appear. The sign of the second derivative of *ρ (∇2ρ)* is analyzed to distinguish attractive and repulsive interactions. The noncovalent interaction regions are represented in the plot as discs with color ranging from blue (attractive) to red (repulsive) as in the VIBGYOR spectrum.

1.5 Hirshfeld Analyses[12, 13]

Important intermolecular interactions within the crystal structure of PYDB-TCNB were identified through Hirshfeld surface analyses using Crystal Explorer 3.1. The Hirshfeld surface is defined as a set of points in 3D space where the ratio of pro molecule and pro crystal electron densities is equal to 0.5. The exploration of intermolecular contacts is provided by mapping normalized contact distances (d_{norm}), which is a function of a closest distance from the point to the nuclei interior (d_i) and exterior (d_e) to the surface as well as on the van der Waals radii (r^{vdw}). 2D fingerprints were generated by deriving from the Hirshfeld surface by plotting the fraction of points on the surface as the function of d_i and d_e, which provide a visual summary of intermolecular contacts within the crystal.

1.6 Symmetry Adapted Perturbation Theory (SAPT)

SAPT(0) analysis was employed to determine the non-covalent interaction energies of dimer molecules. The SAPT module of the psi4[14] code was employed, with 6-31G(d,p) basis set. SAPT(0) calculations provide the contributing components of interaction energy. The results obtained from SAPT(0) analysis is a second order perturbation expansion constituting first order electrostatic and exchange energy parts and second order dispersion, induction and their exchange counterparts as the perturbation terms.

$$E_{int}^{SAPT(0)} = E_{elec}^{(1)} + E_{ex}^{(1)} + E_{ind}^{(2)} + E_{ind-ex}^{(2)} + E_{dis}^{(2)} + E_{dis-ex}^{(2)} \quad \text{(Equation S3)}$$

1.7 Excitonic Coupling Parameters[15, 16]

The excitonic coupling between the donor and acceptor was theoretically examined by evaluating the contributions from both long-range and short-range effects. The values of long-range Coulombic coupling originating from the interaction between molecular transition dipole moments are obtained through the transition charge method using TrESP. The point atomic charges (q) for a monomer are obtained by the transition charge from electrostatic potential (TrESP), and the excitonic coupling corresponds to the Coulomb interaction of transition charges of two monomers:

$$J_{Coul} = \frac{1}{4\pi\varepsilon_o} \sum_{\mathrm{i}} \sum_{j} \frac{q_i q_j}{|r_i - r_j|} \qquad \text{(Equation S4)}$$

where q_i (q_j) represents the transition charge on atom i (atom j) of monomer 1 (monomer 2) in a dimer. Similarly, r_i (r_j) refers to the position vectors of atom i (atom j) of monomer 1 (monomer 2) in a dimer. The TrESP transition charges were obtained from Multiwfn program package.

The short-range exciton coupling stemming from the degree of overlap of wave functions on proximal molecules has a crucial role in defining the excitonic interaction and is determined as,

$$J_{CT} = \frac{-2t_e t_h}{E_{CT} - E_{S_1}} \qquad \text{(Equation S5)}$$

where t_e and t_h are the electron and hole-transfer coupling which depend on the LUMO-LUMO and HOMO-HOMO orbital overlap of the monomers, respectively, E_{CT} is the energy of the charge-transfer state, and E_{S_1} is the energy of the first Frenkel exciton state calculated from TD-DFT. The total coupling between neighbouring molecules can be represented as,

$$J_{Total} = J_{Coul} + J_{CT} \qquad \text{(Equation S6)}$$

1.8 TheoDORE Analysis[16, 17]

The excitations of PYDB-TCNB cocrystal are analyzed using TheoDORE. Here, we considered the donor and acceptor as two different fragments. The parameters used to investigate the excited state characteristics are participation ratio (P_R), mean position (POS) of initial orbital (hole) and final orbital (electron), and charge transfer character (CT). The magnitude of P_R relates to the number of fragments participating in the excitation, hence, in our investigation, the P_R ranges from 1 to 2. POS provides the mean position of hole and electron for a particular excitation. Charge transfer states and delocalized Frenkel states show POS = 1.5. If the Frenkel state is localized on monomer A, then POS = 1, and if localized on monomer B, POS = 2, for a dimer AB. Finally, CT is related to the total weight of configurations where initial and final orbitals are situated on different fragments. A CT value of 1 denotes the presence of a charge-separated state, and CT = 0 refers to Frenkel states. Further, electron-hole correlation plots were generated to analyze the excitonic character of the PYDB-TCNB cocrystal. If the shade is present only in the diagonal parts, the excitonic character is Frenkel. Off-diagonal shades refer to a CT state.

Section B: Syntheses and Characterization

Synthesis of 1,6-Bis(4,4,5,5-tetramethyl-1,3,2-dioxaborolan-2-yl)pyrene

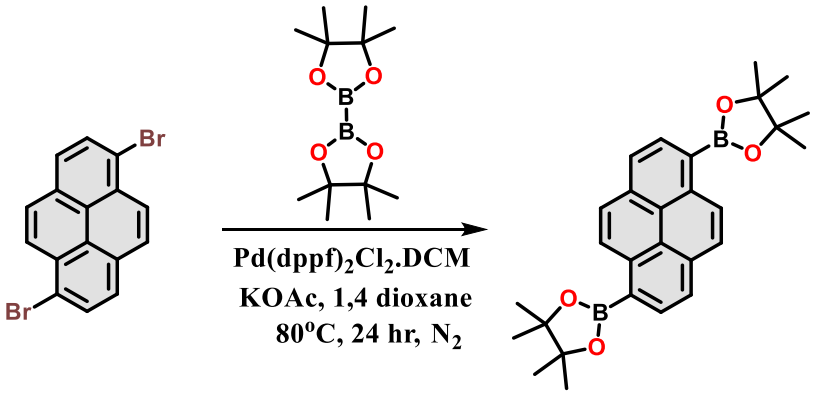

Scheme S1: Shows the synthesis of 1,8-Bis(4,4,5,5-tetramethyl-1,3,2-dioxaborolan-2-yl)pyrene.

In an oven-dried two-neck RB flask, 1,6-dibromo pyrene (0.500 g, 1.38 mmol), bis(pinacolato)diborane (2.8 g, 11.1 mmol, KOAc and $Pd(dppf)_2Cl_2$.DCM (0.096 g, 0.38 mmol) were taken and subjected to high vacuum for 15 min. Dry dioxane (75 mL) was added, and the reaction mixture was allowed to stir at 80 °C for 24 hr under a nitrogen atmosphere. After completion of the reaction, the reaction mixture was cooled to room temperature, following which the organic layer was separated by dichloromethane, and the excess solvent was removed in a vacuum. Further the compound was purified using column chromatography with 10% Ethyl acetate and hexane solvent to yield a white powder in 70% yield. ^{1}H NMR ($CDCl_3$, 500 MHz, 298 K): δ = 9.04 (d, J = 9.2 Hz, 2H), 8.46 (d, J = 7.7 Hz, 2H), 8.12 (d, J = 7.7 Hz, 2H), 8.06 (d, J = 9.2 Hz, 2H), 1.42 (s, 24H). MALDI TOF m/z: $[M]^+$ Calculated for $C_{28}H_{32}B_2O_4$ 454.2487; Found 454.278

Synthesis of PYDB-TCNB cocrystals

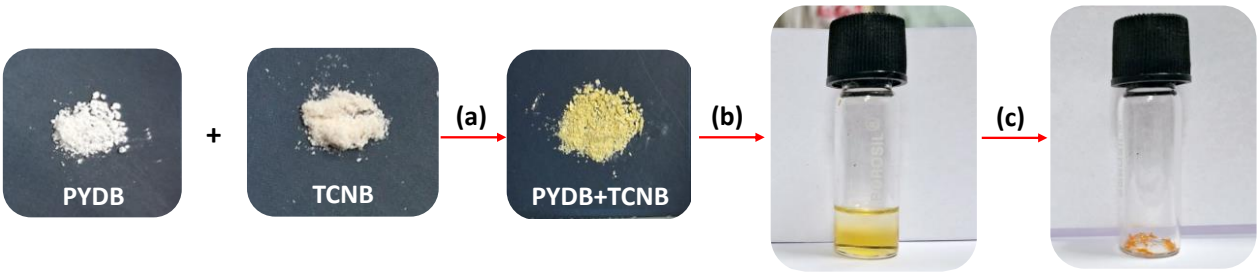

Scheme S2: (a) Add a few drops of methanol to a 1:2 mixture of donor and acceptor grind using the motor and piston. (b) Dissolve in dichloromethane and filter to a vial followed by layering with hexane. (c) Keep it for slow evaporation of solvent for 3-4 days.

The successful CT complexation was achieved by mechanochemical liquid-assisted grinding of PYDB and TCNB with minimal amount of methanol. PYDB and TCNB are mixed in a 1:2 ratio, and a minimal amount of methanol is added. The mixture is thoroughly grinded using a mortar and pestle. During grinding, the white color of the individual donor and acceptor visibly changes to yellow, indicating the formation of a charge transfer (CT) complex. The CT complex is allowed to dry and then transferred to a vial. A saturated solution is prepared using dichloromethane (DCM) as the solvent, and the solution is filtered into another vial. Hexane is then carefully layered over the filtered solution, maintaining a solvent ratio of 2:1 for DCM to hexane. Further, keep it for slow evaporation of the solvent to give nearly 80-85% cocrystals.

Section C: Tables

Table S1: Crystallographic data and refinement parameters for PYDB and PYDB+TCNB.

Parameters	**PYDB**	**PYDB+TCNB**
Formula	$C_{28}H_{32}B_2O_4$	$C_{38}H_{34}B_2N_4O_4$
Formula wt.	454.16	632.31
Crystal system	Monoclinic	Triclinic
Space group,Z	P 21/n	P -1
a, Å	10.5742(7)	6.7950(13)
b, Å	10.9869(8)	10.755(2)
c, Å	11.2991(8)	13.064(2)
α, deg	90	75.068(7)
β, deg	102.084(2)	77.367(7)
γ, deg	90	87.642(7)
V, Å^3	1283.62(16)	900.0(3)
Temp, K	296(2)	296(2)
d_{calcd}, mg/m^3	1.175	1.167
Max. and min. transmission	0.994 and 0.996	0.997 and 0.993
no. of independent reflections	3206	3167
Final R indices [I>2sigma(I)]	R1 = 0.0659	R1 = 0.0697, wR2 = 0.1957
R indices (all data)	wR2 = 0.2197	R1 = 0.1149, wR2 = 0.2345
Goodness of fit on F^2	1.062	1.054
CCDC Deposition number	2393610	2393609

Table S2: Relative % intermolecular interactions obtained from Hirshfeld analysis of PYDB-TCNB cocrystal.

Interaction	%H•••H	%H•••N	%C•••C	%C•••H	%O•••H
PYDB+TCNB	55.0	25.5	8.7	5.9	3.4

Table S3: Interaction energies in selected dimers determined by SAPT(0)/6-31G(d,p) calculations and SAPT(0) energy components for PYDB-TCNB cocrystal.

Dimers	Electrostatic (kJ/mol)	Exchange (kJ/mol)	Induction (kJ/mol)	Dispersion (kJ/mol)	$E^{SAPT(0)}$ (kJ/mol)
DA1	-57.73	71.85	-13.43	-86.29	-85.61
DA2	-6.99	8.40	-1.40	-10.19	-10.20
DA3	-2.59	1.68	-0.37	-3.13	-4.42

Table S4: Temperature-dependent photoluminescence lifetime measurements for PYDB-TCNB cocrystal at ambient and vacuum conditions.

Temperature		τ_1 (ns)	τ_2 (ns)	τ_{avg} (ns)
Room Temperature		11.47 (17.03%)	42.5 (82.97%)	37.2
Under Vacuum	**20 K**	27.16 (19.59%)	82.51 (80.41%)	72.57
	100 K	22.88 (17.46%)	81.51 (82.54%)	71.27
	175 K	24.15 (21.19%)	78.38 (78.81%)	66.88
	250 K	20.35 (19.59%)	66.59 (80.41%)	57.53
	300 K	20.70 (24.28%)	59.14 (75.72%)	49.8

Table S5: Vertical excitation energy (E), mean position (POS), participation ratio (PR), charge transfer character (CT) and exciton character of excited states in PYDB-TCNB at LC-ωhPBE/6-31G(d,p) level of theory.

State	E (eV)	POS	PR	CT
S_1	3.427	1.479	1.049	0.953
S_2	4.034	1.095	1.217	0.169
S_3	4.120	1.081	1.182	0.131
S_4	4.355	1.395	1.421	0.645
S_5	4.339	1.487	1.036	0.965

Section D: Figures

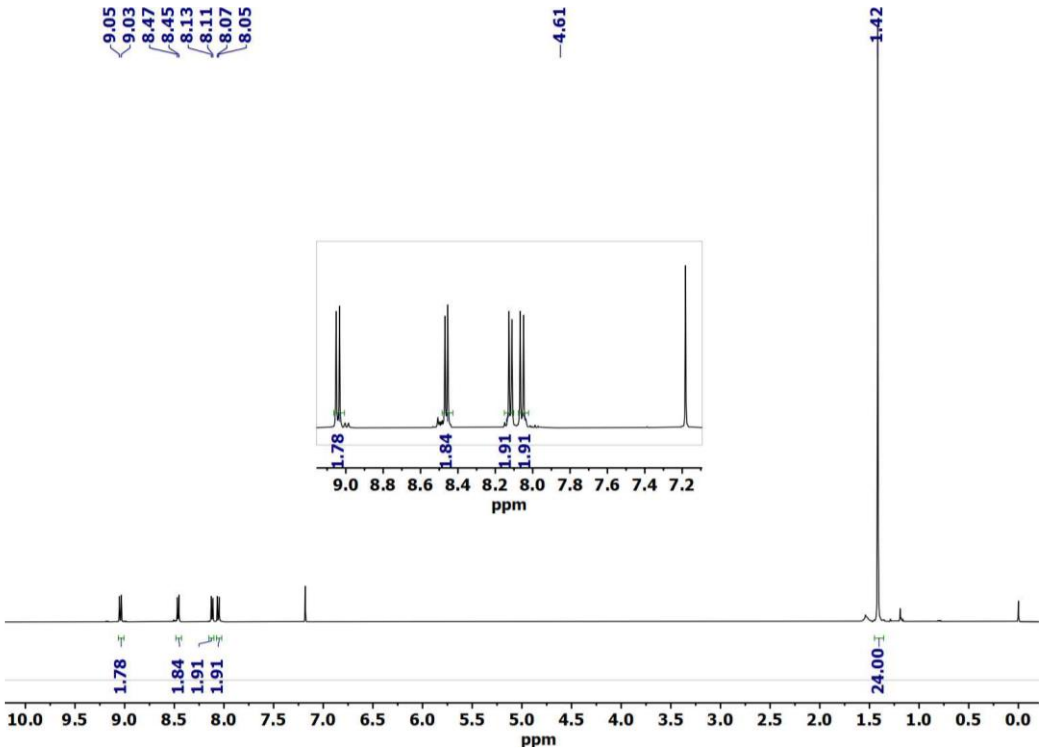

Fig. S1: ^{1}H NMR spectra of PYDB in $CDCl_3$.

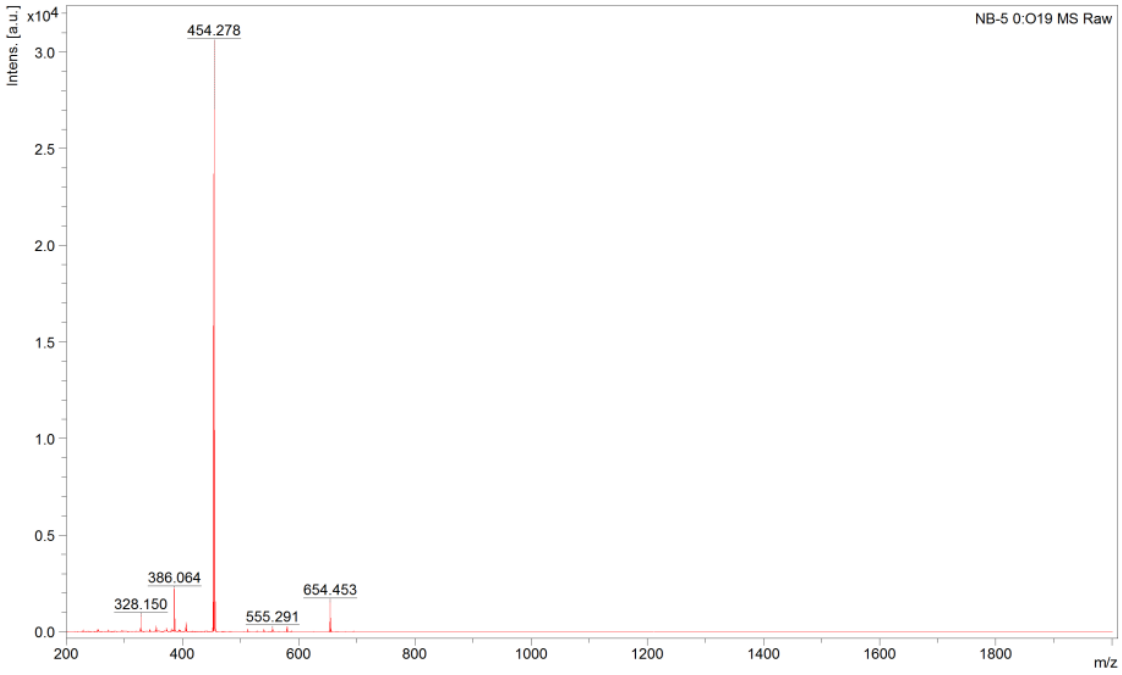

Fig. S2: MALDI-TOF spectrum of spectra of PYDB.

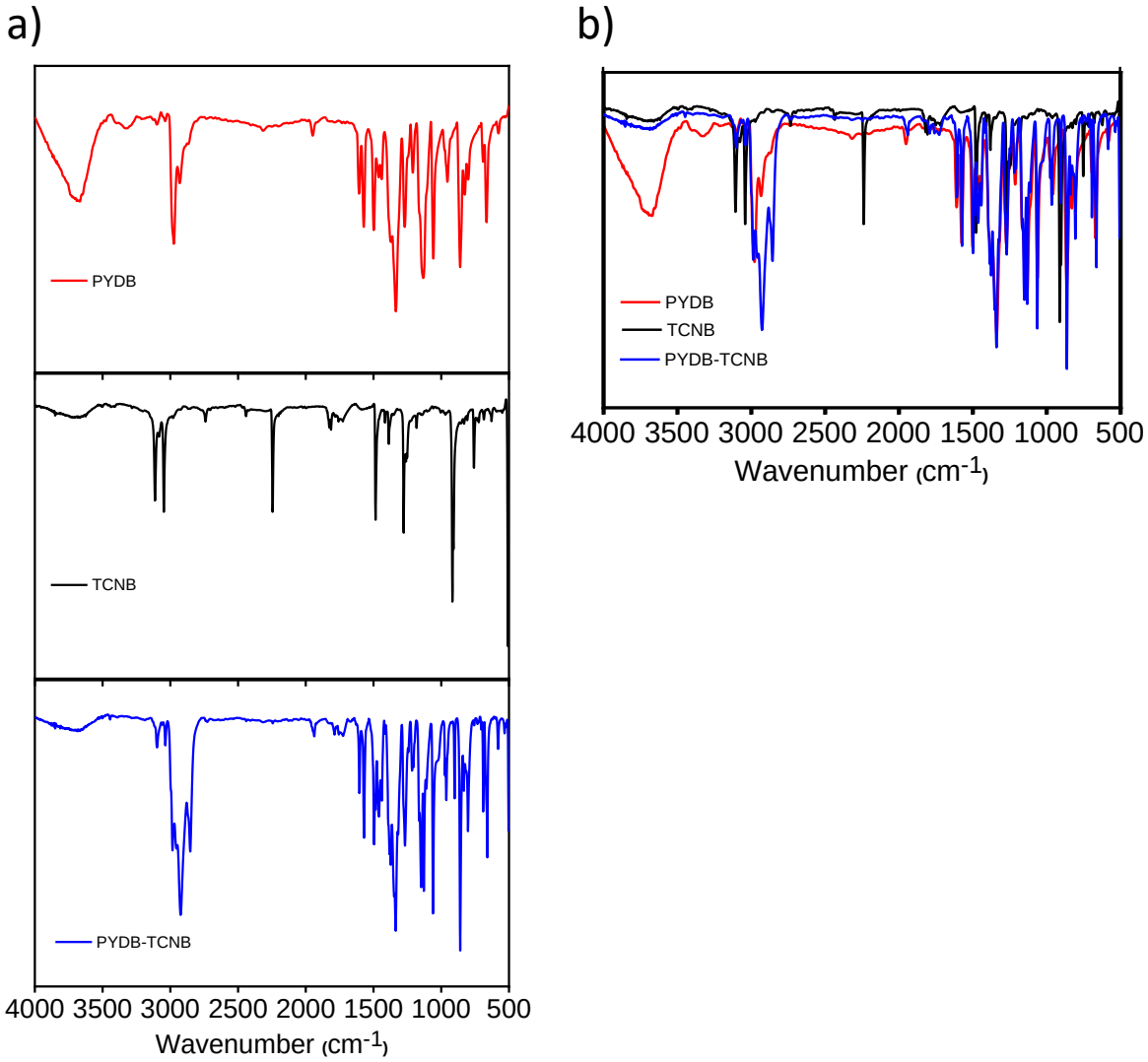

Fig. S3: a) IR spectra of PYDB, TCNB, and PYDB-TCNB b) overlay of PYDB, TCNB, and PYDB-TCNB cocrystal.

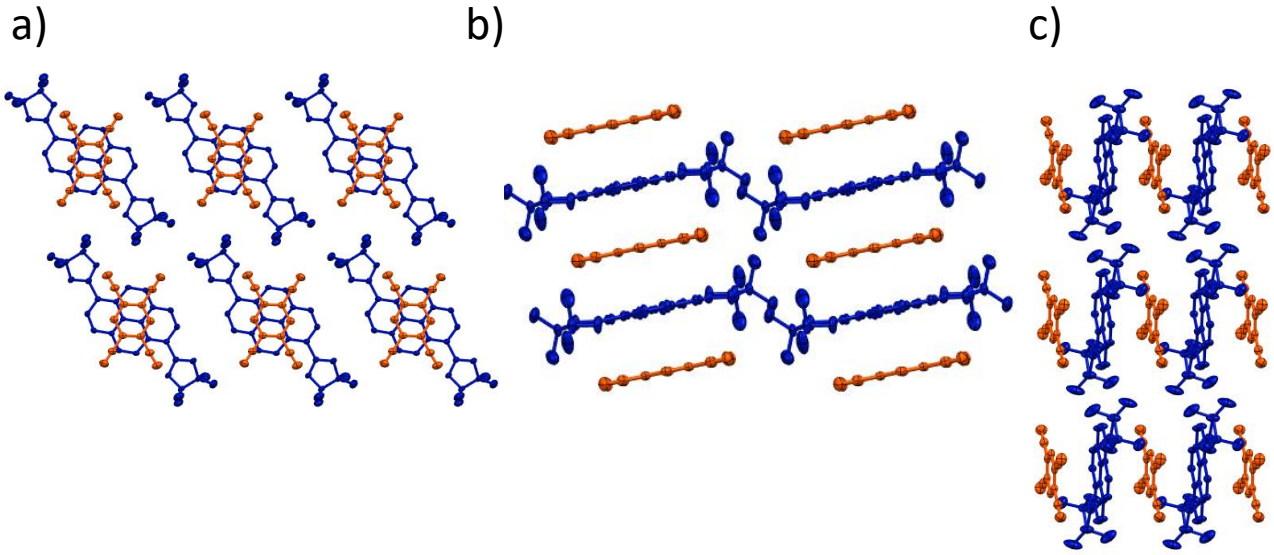

Fig. S4: Crystal packing of PYDB-TCNB viewed along a) a, b) b, and c) c axis, respectively.

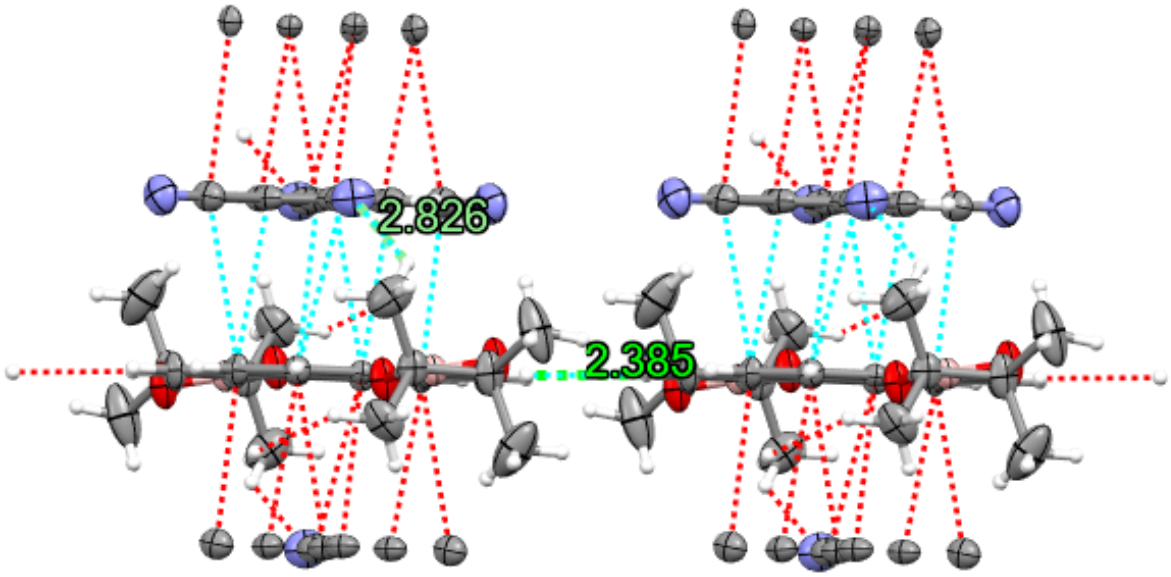

Fig. S5: Additional stabilizing interactions present in PYDB-TCNB cocrystal.

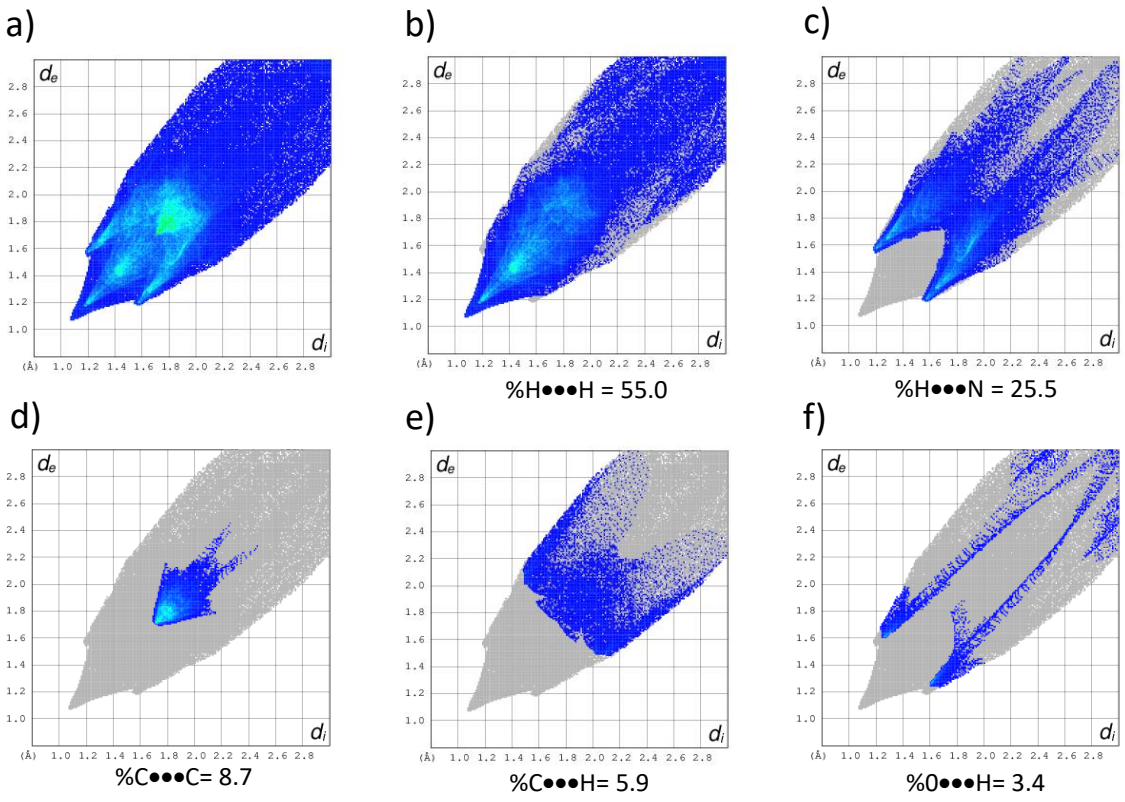

Fig. S6: Hirshfeld 2D fingerprint plots a) Total, b) H•••H, c) H•••N, d) C•••C, e) C•••H and f) O•••H interactions of PYDB-TCNB cocrystal.

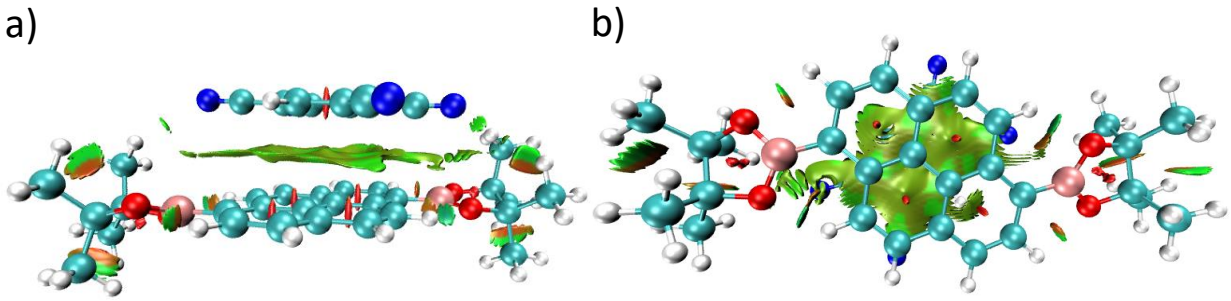

Fig. S7: a) Side view and b) top view of non-covalent interaction (NCI) analysis of PYDB-TCNB cocrystal.

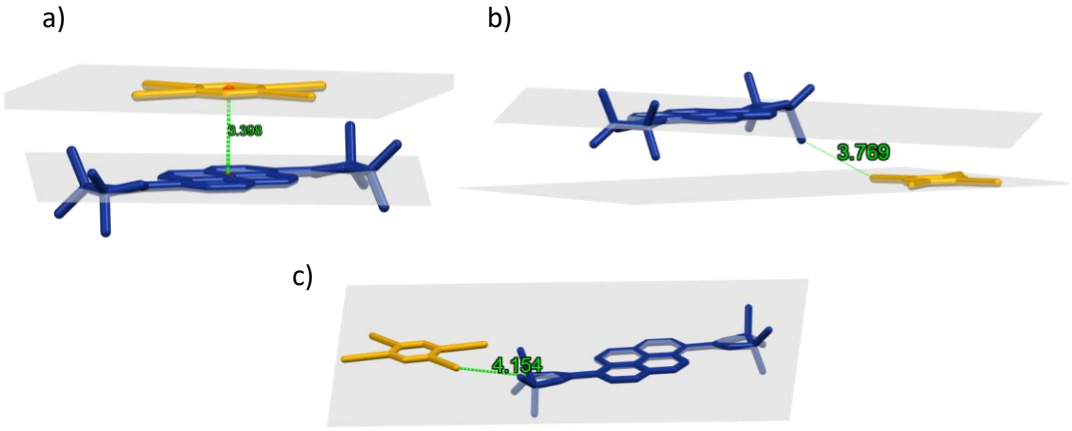

Fig. S8: a) DA1, b) DA2, and c) DA3 dimers of PYDB-TCNB with close contact distance in Å.

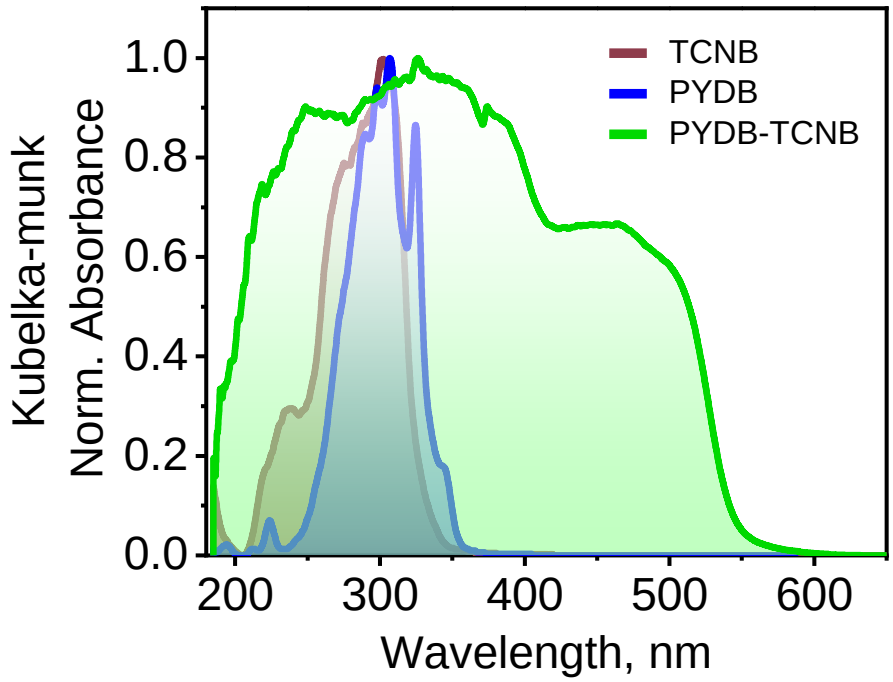

Fig. S9: Normalized Kubelka-Munk diffused reflectance spectra of TCNB (acceptor), PYDB (donor), and PYDB-TCNB (cocrystal).

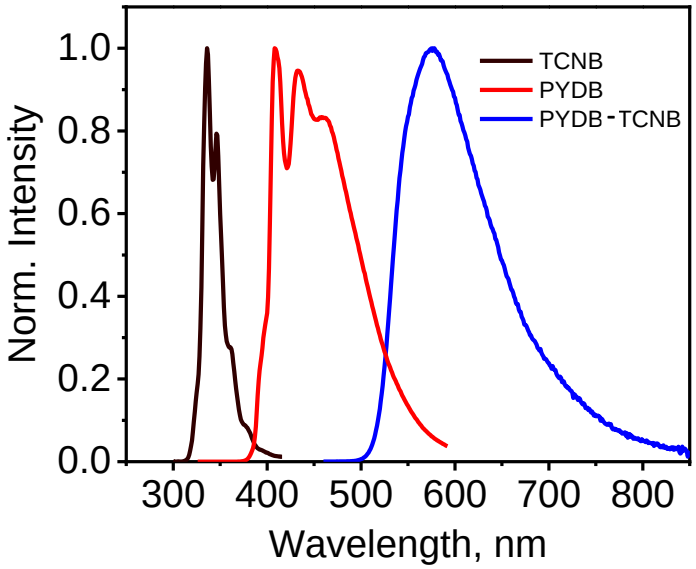

Fig. S10: Steady-state emission spectra of TCNB, PYDB, and PYDB-TCNB cocrystal.

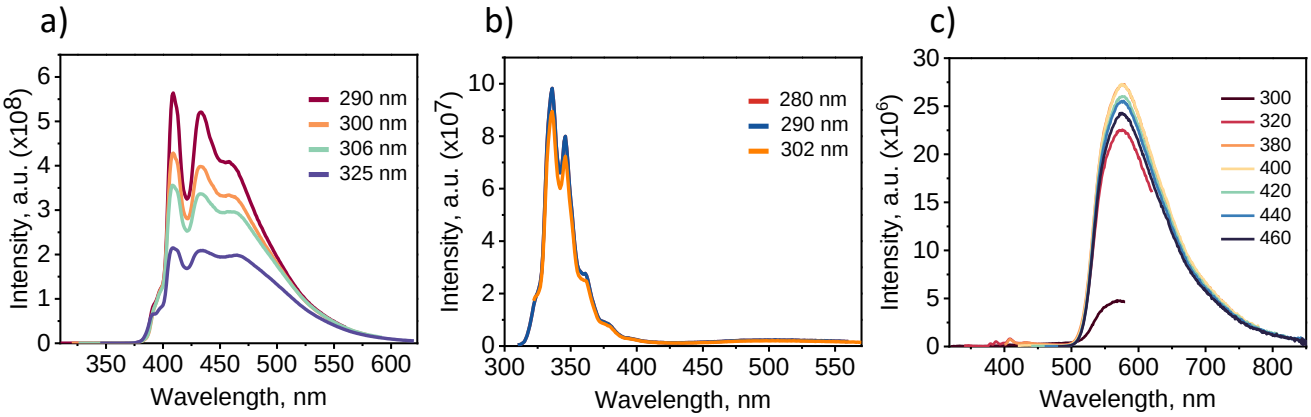

Fig. S11: Excitation-dependent emission spectra of a) PYDB, b) TCNB, and c) PYDB-TCNB cocrystals.

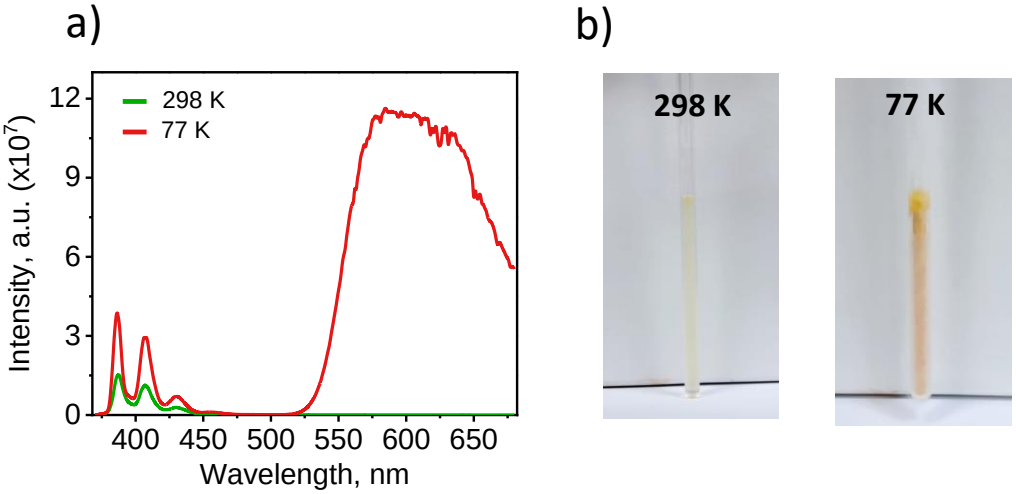

Fig. S12: a) Room temperature and 77 K steady-state emission spectra of PYDB-TCNB cocrystals in dichloromethane solvent. b) Image showing the PYDB-TCNB solution in a quartz tube during two different experimental conditions.

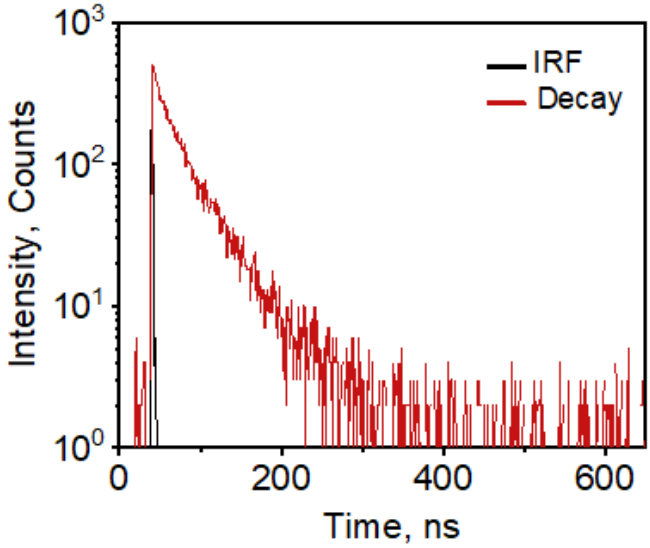

Fig. S13: Photoluminescence lifetime of PYDB-TCNB cocrystal (Recorded at ambient conditions using 340 nm excitation and collecting at 577 nm).

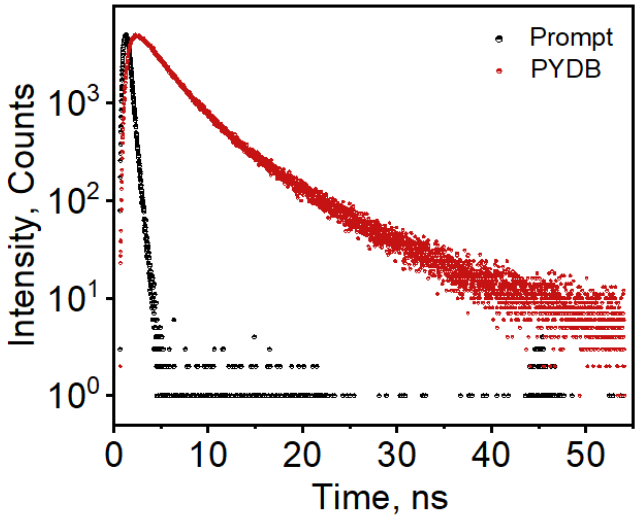

Fig. S14: Photoluminescence lifetime of PYDB (Recorded at ambient conditions using 310 nm excitation).

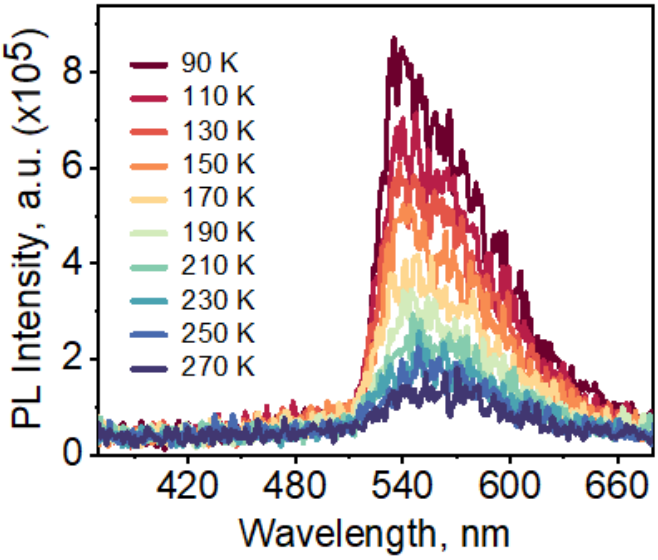

Fig. S15: Temperature-dependent gated emission spectra of PYDB-TCNB cocrystal (Delay time= 50 μs).

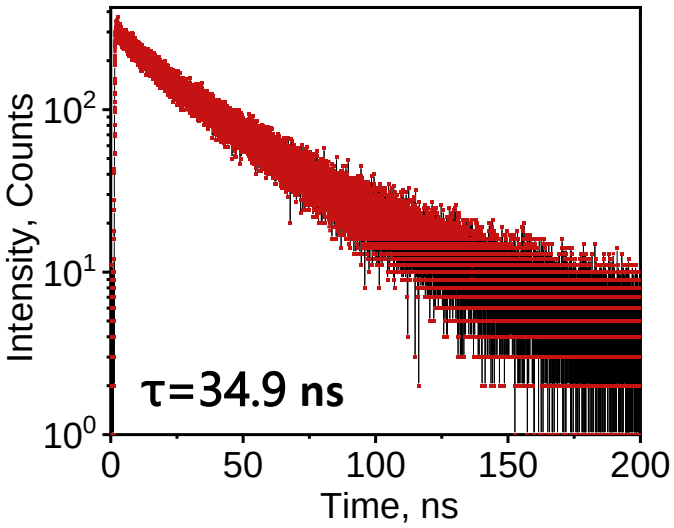

Fig. S16: FLIM fit decay of the PYDB-TCNB cocrystal.

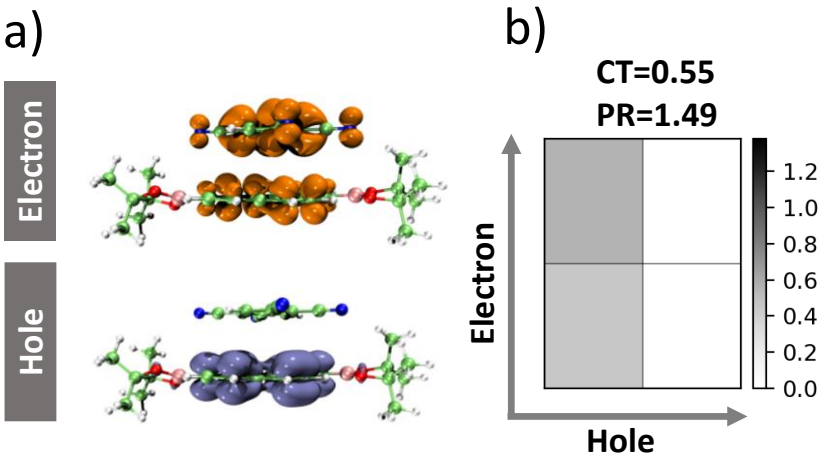

Fig. S17: Electron-hole correlation plots of T_1 state of PYDB-TCNB at LC-ωhPBE/6-31G(d,p) level of theory (isovalue = 0.01).

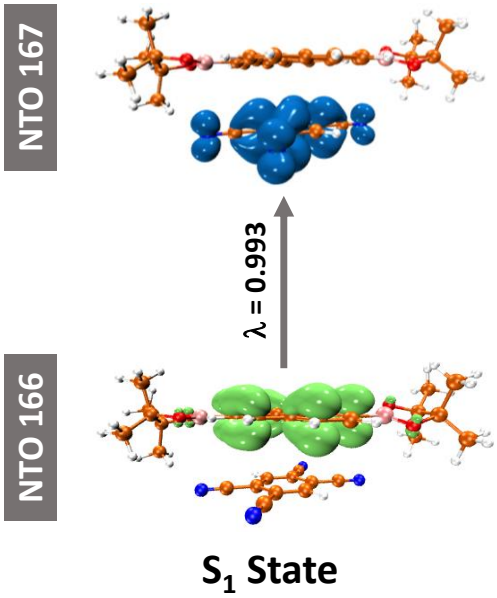

Fig. S18: NTO analysis for S_1 states of PYDB-TCNB cocrystal (isovalue = 0.01).

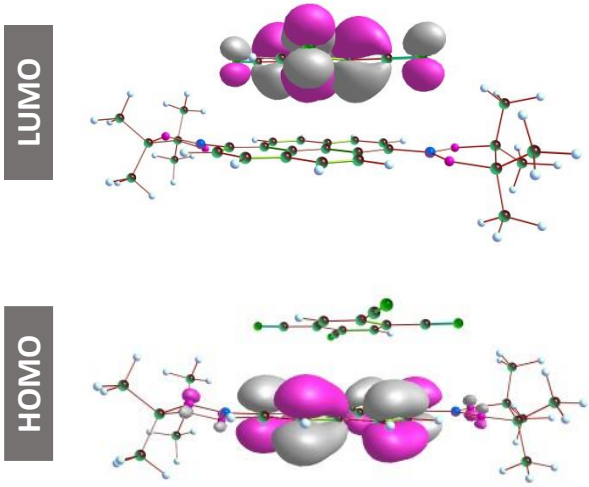

Fig. S19: HOMO and LUMO of PYDB-TCNB cocrystal (isovalue = 0.01).

Coordinates

Optimized ground state geometry of PYDB-TCNB

0 1

O	4.92785100	-1.12734200	-0.68245300
O	5.40391500	1.00880800	-1.31529600
C	1.82588000	-0.38372500	-0.91378400
C	0.49697000	0.08663500	-1.07262000
C	0.26596700	1.40579500	-1.52362400
C	0.96530800	-2.52256000	-0.13124800
H	1.12770700	-3.53131500	0.23789700
C	2.01372000	-1.73619100	-0.44100100
H	3.02710900	-2.10293400	-0.33002600
C	2.91132000	0.47167700	-1.18645400
C	2.64369200	1.77525000	-1.61359200
H	3.48224400	2.43440600	-1.81849700
C	1.35273400	2.23827200	-1.78581100
H	1.17303900	3.25535400	-2.12317200
C	6.35305700	-1.08804800	-0.89830900
B	4.42179200	0.08926900	-1.05162200
C	6.65208900	0.44301500	-0.87009400
C	7.02898100	-1.89156700	0.19618800
H	6.70943500	-1.55996600	1.18426500
H	8.11651800	-1.80519100	0.12422300
H	6.76513700	-2.94604200	0.09138700
C	6.60438700	-1.72250700	-2.26015600
H	6.18084600	-2.72876700	-2.26310500
H	7.67213700	-1.79681000	-2.47807600
H	6.12307100	-1.15008800	-3.05670500
C	6.90393700	0.97819600	0.53376300
H	6.89901200	2.06967300	0.49729900
H	7.87315200	0.65209400	0.91798000
H	6.12631600	0.65425400	1.22895900
C	7.75433900	0.89515800	-1.80966900
H	7.51840100	0.66118400	-2.84791000
H	8.70365700	0.42025000	-1.54797600
H	7.88223300	1.97641400	-1.72690700
O	-5.06465400	0.28764800	-1.42921900
O	-5.50625700	-1.40164200	0.03647100
C	-1.94825800	-0.27379400	-0.88648500
C	-0.62043500	-0.75211900	-0.74900200
C	-0.39037100	-2.05723200	-0.25851600
C	-1.09018800	1.86315700	-1.67422500
H	-1.25171700	2.87774000	-2.02726600
C	-2.13784900	1.07136900	-1.37707600
H	-3.15257700	1.43220600	-1.49644100
C	-3.03235700	-1.09148700	-0.51472500
C	-2.76555300	-2.36569900	-0.00798000
H	-3.60282900	-2.99046100	0.28887200

C	-1.47548000	-2.84823800	0.11403600
H	-1.29587100	-3.84713000	0.50211000
C	-6.46695800	0.39957200	-1.10524000
B	-4.54099400	-0.69995000	-0.63800600
C	-6.77937100	-1.00796300	-0.50994700
C	-7.23006000	0.74133600	-2.37114400
H	-7.02227800	0.02987200	-3.17049800
H	-8.30652700	0.75373800	-2.18049900
H	-6.93602500	1.73441600	-2.71679800
C	-6.59957900	1.52484400	-0.08833300
H	-6.18454500	2.43900000	-0.51753200
H	-7.64549300	1.71039800	0.16670300
H	-6.04380300	1.30803800	0.82598000
C	-7.13734600	-2.04026300	-1.57209900
H	-7.13642300	-3.03117200	-1.11357500
H	-8.12732500	-1.85664400	-1.99554300
H	-6.40482300	-2.04117300	-2.38287800
C	-7.81135500	-1.01595400	0.60159400
H	-7.49380000	-0.40089800	1.44358600
H	-8.77401700	-0.64656000	0.23817400
H	-7.95314600	-2.03735400	0.96088800
C	-0.13706500	2.12951300	1.85230000
C	1.49255400	0.45029600	2.40506100
N	-0.65070500	4.52602800	1.01113000
C	-0.43406500	3.45561600	1.38321200
C	1.18765000	1.72647300	1.95169400
H	1.98265900	2.40205800	1.65959500
C	2.87131600	0.05587000	2.50846000
N	3.98509200	-0.23175000	2.59586600
C	0.46503700	-0.43538300	2.75075800
C	-1.16456000	1.24546500	2.20200200
N	0.97550000	-2.82754400	3.60599800
C	0.76095100	-1.76225600	3.21832700
C	-0.85985300	-0.03527600	2.64261300
H	-1.65683400	-0.72712300	2.88828400
C	-2.54299000	1.64387900	2.11451400
N	-3.65597600	1.94403700	2.07114800

References

1. Y. Zhang, J. Sun, G. Zhuang, M. Ouyang, Z. Yu, F. Cao, G. Pan, P. Tang, C. Zhang and Y. Ma, *J. Mater. Chem. C*, 2014, **2**, 195-200.
2. J. Gierschner, S. Varghese and S. Y. Park, *Adv. Opt. Mater.*, 2016, **4**, 348-364.
3. G. M. Sheldrick, *Acta Crystallogr. A*, 2008, **64**, 112-122.
4. A. Spek, *J. Appl. Crystallogr.*, 2003, **36**, 7-13.
5. L. Farrugia, *J. Appl. Crystallogr.*, 1999, **32**, 837-838.
6. I. J. Bruno, J. C. Cole, P. R. Edgington, M. Kessler, C. F. Macrae, P. McCabe, J. Pearson and R. Taylor, *Acta Crystallogr. B*, 2002, **58**, 389-397.
7. C. F. Macrae, I. J. Bruno, J. A. Chisholm, P. R. Edgington, P. McCabe, E. Pidcock, L. Rodriguez-Monge, R. Taylor, J. van de Streek and P. A. Wood, *J. Appl. Crystallogr.*, 2008, **41**, 466-470.
8. Gaussian 09, Revision A.02, M. J. Frisch, G. W. Trucks, H. B. Schlegel, G. E. Scuseria, M. A. Robb, J. R. Cheeseman, G. Scalmani, V. Barone, G. A. Petersson, H. Nakatsuji, X. Li, M. Caricato, A. Marenich, J. Bloino, B. G. Janesko, R. Gomperts, B. Mennucci, H. P. Hratchian, J. V. Ortiz, A. F. Izmaylov, J. L. Sonnenberg, D. Williams-Young, F. Ding, F. Lipparini, F. Egidi, J. Goings, B. Peng, A. Petrone, T. Henderson, D. Ranasinghe, V. G. Zakrzewski, J. Gao, N. Rega, G. Zheng, W. Liang, M. Hada, M. Ehara, K. Toyota, R. Fukuda, J. Hasegawa, M. Ishida, T. Nakajima, Y. Honda, O. Kitao, H. Nakai, T. Vreven, K. Throssell, J. A. Montgomery, Jr., J. E. Peralta, F. Ogliaro, M. Bearpark, J. J. Heyd, E. Brothers, K. N. Kudin, V. N. Staroverov, T. Keith, R. Kobayashi, J. Normand, K. Raghavachari, A. Rendell, J. C. Burant, S. S. Iyengar, J. Tomasi, M. Cossi, J. M. Millam, M. Klene, C. Adamo, R. Cammi, J. W. Ochterski, R. L. Martin, K. Morokuma, O. Farkas, J. B. Foresman, and D. J. Fox, Gaussian, Inc., Wallingford CT, 2016.
9. T. Lu and F. Chen, *J. Comput. Chem.*, 2012, **33**, 580-592.
10. GitHub - JoshuaSBrown/QC_Tools: This small repository provides functionality for calculating the charge transfer integrals between two molecules. https://github.com/JoshuaSBrown/QC_Tools (accessed Apr 15, 2020).
11. J. Contreras-García, E. R. Johnson, S. Keinan, R. Chaudret, J.-P. Piquemal, D. N. Beratan and W. Yang, *J. Chem. Theory Comput.*, 2011, **7**, 625-632.
12. S. K. Rajagopal, A. M. Philip, K. Nagarajan and M. Hariharan, *Chem. Commun.*, 2014, **50**, 8644-8647.

13. M. A. Spackman and D. Jayatilaka, *CrystEngComm*, 2009, **11**, 19-32.
14. R. M. Parrish, L. A. Burns, D. G. A. Smith, A. C. Simmonett, A. E. DePrince, III, E. G. Hohenstein, U. Bozkaya, A. Y. Sokolov, R. Di Remigio, R. M. Richard, J. F. Gonthier, A. M. James, H. R. McAlexander, A. Kumar, M. Saitow, X. Wang, B. P. Pritchard, P. Verma, H. F. Schaefer, III, K. Patkowski, R. A. King, E. F. Valeev, F. A. Evangelista, J. M. Turney, T. D. Crawford and C. D. Sherrill, *J. Chem. Theory Comput.*, 2017, **13**, 3185-3197.
15. N. J. Hestand and F. C. Spano, *J. Chem. Phys.*, 2015, **143**, 244707.
16. F. Plasser and H. Lischka, *J. Chem. Theory Comput.*, 2012, **8**, 2777-2789.
17. F. Plasser, *J. Chem. Phys.*, 2020, **152**, 084108.